Hydrogen Bonded Assembly of Poly(acrylic acid)-*block*-poly(L-valine) in Dilute Solutions

A. Sinaga,[†] T. A. Hatton,[‡] and K. C. Tam*[,§]

Singapore−MIT Alliance, National University of Singapore, E4-B-07/8, 4 Engineering Drive 3, Singapore 117576, Department of Chemical Engineering, Massachusetts Institute of Technology, Cambridge, Massachusetts 02139, and Department of Chemical Engineering, University of Waterloo, 200 University West Avenue, Ontario, Canada N2L 3G1

Received July 11, 2007; Revised Manuscript Received August 27, 2007

ABSTRACT: The self-assembly of four hybrid poly(acrylic acid)-*block*-poly(L-valine) (PAA-*b*-PLVAL) block copolymers (i.e., PAA_{40}−$PLVAL_{100}$, PAA_{80}−$PLVAL_{100}$, PAA_{80}−$PLVAL_{80}$, and PAA_{80}−$PLVAL_{60}$) was investigated. Formation of core−shell spherical micelles was observed, and it correlated with the extent of β-sheet ordering in PLVAL hydrophobic domains. PAA_{80}−$PLVAL_{60}$, having the lowest β-sheet content (12%), existed only as random aggregates at pH < 5 and in an unaggregated state at high pH. The β-sheet formation also produced an unusual pH dependence of the micelles, where the swelling of micelles occurred only within a narrow degree of deprotonation (α) range of between 0.15 to 0.2 and 0.4 to 0.5 for PAA_{80}−$PLVAL_{80}$ and PAA_{80}−$PLVAL_{100}$, respectively. An additional role of the length of the PAA segment was identified as providing sufficient shielding to the hydrophobic core, which prevents further association into large compound micelles, as was observed for PAA_{40}−$PLVAL_{100}$.

Introduction

Block copolymers composed of segments with incompatible chemical and physical properties will spontaneously self-assemble into ordered structures of sub-micrometer size that are attractive for a variety of applications, such as drug/DNA delivery,[1,2] liquid crystalline materials,[3] and emulsifying agents.[4] The three basic morphologies commonly found are spherical, cylindrical, and vesicle-like micellar structures.[5] These three basic shapes differ in terms of curvature between condensed phase (micellar core) and extended phase (corona), where the highest curvature is found for spherical particles. For most conventional copolymer systems, the difference in solubility in aqueous solution (hydrophobicity) is the main driving force for self-assembly, and the overall size and shape of the ordered structure are determined by the volume fractions of different blocks and environmental factors, such as solvent polarity, ionic strength, pH, and temperature.[6]

Preparation of hybrid systems between conventional synthetic polymers (PEO, polybutadiene, PLA, etc.) and linear sequences of amino acids are interesting because amino acid segments possess unique properties, such as directional polarity and chirality[7,8] and their capability to undergo specific noncovalent interactions (secondary structure effects). These properties can potentially be used for designing novel hierarchical superstructures with tunable material properties for a wide variety of applications. Furthermore, conformational transitions of amino acid segments between different secondary structures (α-helix, β-sheet, and random coil) provide alternatives in the preparation of smart and responsive materials toward a variety of different environmental stimuli, such as pH and temperature changes.[9−11]

The simplest class of polypeptide hybrid systems is one with a multiblock architecture with sequential arrangements of polypeptides and synthetic polymer blocks. These peptide hybrid block copolymers can be classified based on the relative solubility of the peptide and synthetic segments. Charged polypeptides, such as poly(L-lysine), poly(L-aspartic acid), etc., are corona-forming polypeptides due to their excellent aqueous solubility, while hydrophobic peptides, such as poly(L-leucine) and poly(L-alanine), are core-forming. The effects of secondary structure on aggregation behavior, however, are generally more pronounced for the latter. Also, incorporation of β-sheet secondary structural motifs is particularly advantageous since it may impart excellent mechanical properties to the material through the formation of well-orientated crystalline fillers similar to natural silks.[12,13] Preparation of β-sheet containing materials is generally complicated by the intractable nature of the β-sheet component, which can only be dissolved in polar organic solvents (e.g., hexafluoro-2-propanol), and hence, they have been used mostly in film-casting applications and only very limited aqueous-based applications.[14−16] Strategies to improve the aqueous solubility of such β-sheet containing materials are therefore important.

In this paper, the aqueous self-assembly behavior of hybrid block copolymers between poly(acrylic acid) (PAA) and a β-sheet forming poly(L-valine) (PLVAL) will be described for polymers of four different compositions, namely, PAA_{40}−$PLVAL_{100}$, PAA_{80}−$PLVAL_{100}$, PAA_{80}−$PLVAL_{80}$, and PAA_{80}−$PLVAL_{60}$. Previously, the formation of water-soluble β-sheet structures was observed for polymeric systems with a total β-sheet content of between 30 and 60%, depending on polymer composition and pH.[17] The block copolymers were observed to preferentially form core−shell spherical micelles rather than lamellar or fibrillar arrangements, possibly due to the much higher entropy loss in the latter two structures. The extent of secondary β-sheet formation by PLVAL correlated with the shape regularity of the self-assembled morphology that also resulted in a pH swelling behavior that is typical of cross-linked systems with a constant micellar size over a wide range of α. In addition, the length of PAA segment was observed to be

* Corresponding author. Fax: (519) 746-4979; e-mail: mkctam@uwaterloo.ca.
[†] National University of Singapore.
[‡] Massachusetts Institute of Technology.
[§] University of Waterloo.

10.1021/ma071539l CCC: $37.00
Published on Web 11/08/2007

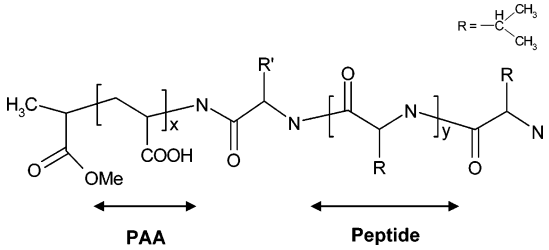

Figure 1. Chemical structure of PAA-*b*-PLVAL.

Table 1. Molecular Composition and PDI of PAA-*b*-PLVAL

polymer	*X*	*y*	MW[a]	PDI[b]	% hydrolysis[c]
1	80	100	15 600	1.18	96.2
2	80	80	13 700	1.21	95.3
3	80	60	11 700	1.17	94.1
4	40	100	12 800	1.24	97.1

[a] MW was obtained from NMR in d_7-DMF. [b] PDI was determined from GPC of the corresponding poly(*t*BA)-PLVAL prior to hydrolysis: column temperature, 60 °C; eluent, 1% LiBr in DMF; and elution rate, 1 mL/min. [c] % hydrolsis determined from the acid−base potentiometric titration.

important for the colloidal stability of particles and also to prevent the formation of large compound micelles as in the $PAA_{40}-PLVAL_{100}$ systems.

Experimental Procedures

Materials. Four PAA-*b*-PLVAL copolymers were synthesized through the combined approach of ATRP, click chemistry, and nickel-catalyzed polymerization of *N*-carboxyanhydrides of L-valine as described previously.[18] The chemical structure of the block copolymers is shown in Figure 1, while the composition, polydispersity index (PDI), and percent hydrolysis are summarized in Table 1. The percent hydrolysis refers to the percent conversion of the deprotected reaction that generates COOH groups from the initial *t*-butyl acrylate protecting groups. As can be observed in Table 1, the percent hydrolysis of all copolymers was greater than 94%, and hence, we would expect minimal contribution from the hydrophobic *t*-butyl acrylate group toward the self-assembly of the block copolymers.

Sample Preparation. Prior to preparing the test solutions, the block copolymer obtained from the synthesis was additionally purified by dialysis in deionized water. Typically, polymers were dissolved in deionized water at a concentration of 0.5 wt % and transferred into a regenerated cellulose dialysis membrane (Snake Skin Pleated Dialysis Tubing) having a molecular weight cutoff of 3500 Da. Dialysis was carried out for 1 week with the deionized water replaced every half day. The polymers were then freeze-dried to yield a white powder that was easily redispersed in deionized water. Polymer stock solutions of 1 wt % were then prepared and stored in a freezer. Test solutions with pH of between 5 and 10 and concentrations of 0.02−0.12 wt % were subsequently prepared by diluting the stock solution with pre-filtered deionized water (with a 0.2 μm nylon membrane filter). The solutions were adjusted to a final NaCl salt concentration of 0.2 M using a 2 M NaCl stock solution. All samples were equilibrated overnight prior to physical characterizations to ensure that the self-assembly process had reached equilibrium.

Instrumentation. Potentiometric Titration. An ABU93 Triburette Titration System equipped with Radiometer pHG201 pH glass and Radiometer REF201 reference electrodes was used to conduct potentiometric and conductometric titrations. All titrations were performed under constant stirring at 25 °C, in a 100 mL titration vessel. Polymer solutions were prepared at a concentration of 0.1 wt % and pH of 10. The 1 M standard HCl and NaOH solutions (from Merck) were then used for the forward acid and backward base titrations. A lag time of 1 min was allowed between two consecutive dosages to ensure that the neutralization reaction had reached equilibrium.

Laser Light Scattering. The dynamic (DLS) and static (SLS) laser light scattering experiments were conducted using a Brookhaven laser light scattering system. This system consists of a BI200SM goniometer, BI-9000AT digital correlator, and other supporting data acquisition and analysis software and accessories. An argon ion vertically polarized 488 nm laser was used as the light source. The concentration of the polymer solutions investigated by light scattering was kept within the dilute solution regime (0.02−0.12 wt %), where the behavior of individual particles can be characterized. Furthermore, 0.2 M NaCl was added to the solution to screen interparticle electrostatic repulsions that may contribute to errors in the measurement of particle sizes. All samples were passed through a 0.45 μm nylon filter membrane prior to measurement to remove dust. In DLS, the intensity of scattered light was measured as a function of time, and the time correlation function of the scattered intensity ($G2(t)$), defined as $G2(t) = I(t)I(t + \Delta t)$, where $I(t)$ is the intensity at time t and Δt is the lag time, was analyzed using the inverse Laplace transformation technique (REPES) to produce the distribution function of decay times. Several measurements were performed at varying scattering angles (60−120°) for a given sample to confirm that translational diffusion was the main mode of particle motion that gave rise to the observed DLS peak and hence justifying the use of the Stokes−Einstein equation to calculate the average hydrodynamic radius. In SLS, the time-averaged intensity of scattered light was measured at different scattering angles, and the results were plotted in the form of Berry plots to obtain molecular weight, second virial coefficient (A_2), and radius of gyration (R_g) of the polymer aggregates.

Transmission Electron Microscopy (TEM). Transmission electron microscopic images were obtained using a JEOL JEM-2010 transmission electron microscope operating at an acceleration voltage of 200 kV. A Formvar-carbon precoated copper grid was placed on filter paper, and a 0.1 wt % polymer solution was placed on it and air-dried. A drop of 0.1% solution of phosphotungstic acid in ethanol was then added to stain the polymer aggregates. The copper grid was immersed in liquid nitrogen and immediately dried overnight in a freeze drier prior to measurement.

Zeta Potential. The colloidal stability and surface charge of the polymer aggregates were examined at room temperature using a Brookhaven ZetaPlus analyzer. Each run in the sample measurements consisted of five cycles where the charges on the two electrodes were alternated and an average reading from five runs was used to obtain the particle electrophoretic mobility. A Smoluchowsky approximation, which is applicable for particles with diameters equal to or larger than 0.2 μm in a solvent with a high dielectric constant, was subsequently used to calculate the zeta potential of the particles.

Surface Tension. A DCAT21 dynamic contact angle meter and tensiometer was used together with a Wilhelmy plate to measure the surface tension changes during the addition of a concentrated polymer stock solution (1 wt %) into water at room temperature. A plot of surface tension with polymer concentration allows the determination of the critical micellar concentration (cmc) of the polymer at a particular pH and ionic strength.

Results and Discussion

cmc of Self-Assembled Morphology. An important property describing the self-assembly behavior of aqueous solutions of block copolymers is the cmc, which is the minimum concentration where the copolymers self-assemble into micellar aggregates. This critical concentration is usually described by a sharp change in the plot of different solution properties as a function of concentration (i.e., surface tension, viscosity, turbidity, etc.). Plots of the surface tension as a function of concentration for the four different PAA-*b*-PLVAL copolymers at a pH of 10 are shown in Figure 2A, with the cmc determined from the intercept of two linear regions of the plot. The surface tension plot generally showed a typical micellization behavior, where a sharp reduction in the surface tension occurred at

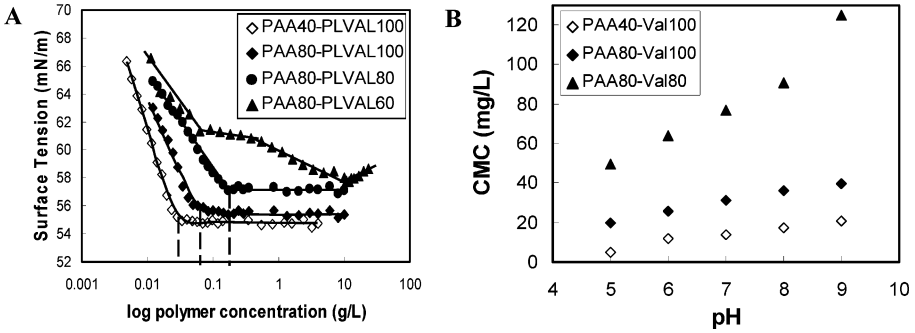

Figure 2. Determination of cmc of PAA-*b*-PLVAL by surface tension measurements. (A) Surface tension plot of PAA-*b*-PLVAL at pH 10 and (B) dependence of cmc on pH.

concentrations below the cmc due to the localization of polymer molecules on the air−water interface followed by a constant surface tension region above the cmc after the air−water interface was fully saturated. The polymer molecules at this stage would aggregate to minimize unfavorable contacts between the hydrophobic PLVAL segment and water molecules to reduce its free energy. As can be observed from Figure 2A, the effect of increasing the PLVAL composition in the copolymer was to increase the aggregation tendency of the system, which shifted the cmc to a lower concentration.

The surface tension of $PAA_{80}-PLVAL_{60}$ in Figure 2A indicated a different association process from the other three polymers, where the cmc of $PAA_{80}-PLVAL_{60}$ was not well-defined and the surface tension decreased in two stages. The first stage was a sharp reduction followed by a gradual decrease that spanned a broad concentration regime (0.1−1 g/L). This gradual decrease indicated that there was no preferred localization of polymer molecules toward the air−water interface and that the formation of polymer aggregates commenced before the surface was saturated, possibly because the PLVAL segment was not as hydrophobic as the other three polymers. The second stage was between 1 and 10 g/L, where there was a further steeper decline of the surface tension, although not as steep as the first stage. In this region, small polymer aggregates with a more efficient packing than individual polymer chains partitioned to the air−water interface, allowing for a higher surface coverage and reduction of the surface tension. It can also be noted that the surface tension of $PAA_{80}-PLVAL_{60}$ increased at concentrations greater than 10 g/L prior to precipitation. This increase in the surface tension may be due to a subsequent association of small polymer aggregates into larger aggregates, resulting in depletion of the surface concentration. Therefore, we concluded that PAA_{80}-*b*-$PLVAL_{60}$ underwent a random association process, while the other three copolymers displayed a conventional cooperative association process. For this reason, subsequent investigation of the self-assembly behavior will not include $PAA_{80}-PLVAL_{60}$.

The effect of increasing pH on the cmc of the three copolymers is shown in Figure 2B, where the aggregation of the copolymers occurred at an increasingly higher cmc at higher pH. An increase in the pH resulted in the neutralization/deprotonation of COOH groups on PAA segments that imparted increasing amounts of negative charges on the polymer. These charges stabilized the polymer in the form of individual unimers as electrostatic repulsion between polymer molecules presented a barrier toward micellization.

Potentiometric Titration of PAA-*b*-PLVAL. The presence of PAA segment in the block copolymer systems imparts responsiveness of the self-assembly process to changes in the solution pH. An important parameter that varies with the pH is the degree of charge density on the polymeric chains, brought about by the neutralization of some COOH to COO^- groups. Hence, the charge density will be directly proportional to the degree of neutralization/deprotonation, α, of the polymer. This α parameter was obtained from acid−base potentiometric titration and is defined as the fraction of total COOH groups present in its deprotonated form (COO^-) as defined by eq 1. COOH groups are weak acids that dissociate in aqueous solutions as described by the equilibrium in eq 2 and an acid dissociation constant defined by eq 3

$$\alpha = \frac{[COO^-]}{[COOH]_{total}} \tag{1}$$

$$[COOH] \leftrightarrow [COO^-] + [H^+] \tag{2}$$

$$K_a = \frac{[COO^-][H^+]}{[COOH]} \tag{3}$$

Since the self-assembly of charged polymers is dependent on its charge density, comparison of different polymers is more suitably done at the same α. To facilitate this, the potentiometric titration data can be used to obtain the relationship between pH and α or vice versa. Figure 3A shows the pH−α curves for the four polymers. It was observed that as the length of PAA segment was increased relative to PLVAL segment, an increasingly higher pH was required to achieve the same degree of ionization, indicating an increased resistance to the proton dissociation process.[17] More information and insights on the morphological changes with pH of the solution can be gained from the dependence of the apparent dissociation constant (pK_a) of various polymers on α. This is because the pK_a parameter is essentially a measure of the ease of proton dissociation, and its magnitude is sensitive to both changes in the overall charge density of the polymer and the local microenvironment surrounding the COOH groups. The pK_a of the polymers can be calculated from the Henderson−Hasselbalch equation (eq 4), derived from the definition of α (eq 1) and equilibrium dissociation constant (eq 3), and the results were plotted in Figure 3B for the four block copolymers

$$pK_a = pH + \log\frac{1-\alpha}{\alpha} \tag{4}$$

As can be observed from Figure 3, the polymer with the lowest valine content (i.e., $PAA_{80}-PLVAL_{60}$) exhibited the lowest pK_a at all ranges of α, where the pK_a increased linearly with increasing α. This is a typical behavior observed for linear PAA homopolymers, where the increase in the apparent pK_a at high α is due to the enhanced electrostatic forces of the polymer

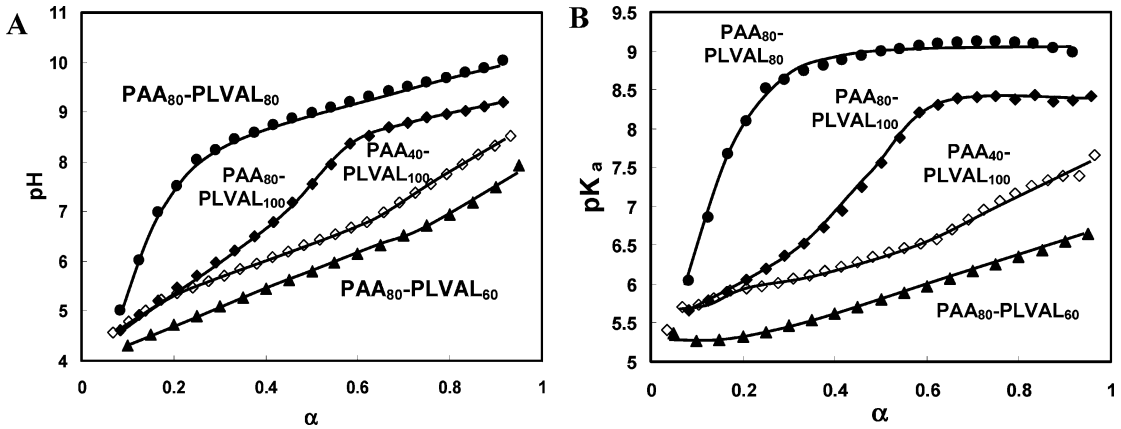

Figure 3. Potentiometric titration analysis of PAA-*b*-PLVAL systems. (A) Comparison of pH−α curves for PAA_{40}−$PLVAL_{100}$, PAA_{80}−$PLVAL_{100}$, PAA_{80}−$PLVAL_{80}$, and PAA_{80}−$PLVAL_{60}$ and (B) Comparison of pK_a−α curves for PAA_{40}−$PLVAL_{100}$, PAA_{80}−$PLVAL_{100}$, PAA_{80}−$PLVAL_{80}$, and PAA_{80}−$PLVAL_{60}$.

from the increased concentration of COO^- groups, which hindered further dissociation of H^+. There was no observable effect of the PLVAL segment on the proton dissociation behavior of this polymer.

For the other PAA_{80}−$PLVAL_y$ (y = 80, 100) and PAA_{40}−$PLVAL_{100}$ systems, the pK_a did not increase linearly at all ranges of α. For example, plateaus in the pK_a−α curves can be observed at α = 0.2−0.5, α > 0.3, and α > 0.6 for PAA_{40}−$PLVAL_{100}$, PAA_{80}−$PLVAL_{80}$, and PAA_{80}−$PLVAL_{100}$, respectively. The pK_a values at any given α for these systems were also found to be significantly higher as compared to the PAA_{80}−$PLVAL_{60}$ system. In these systems, the PLVAL segments were observed to present an additional barrier toward proton dissociation that was possibly attributed to the inaccessibility of the COOH groups. A similar observation was reported by Wang et al., where the pK_a of a random copolymer was found to be higher than the pK_a of a block copolymer with similar MAA/EA composition at low α due to the entrapment of COOH groups inside a compact latex particle.[19] Comparing the PAA_{80}−$PLVAL_y$ (y = 80, 100) and PAA_{40}−$PLVAL_{100}$ systems, a correlation existed where a reduction in the PLVAL/PAA molar ratio resulted in an increase in the deprotonation barrier.

The potentiometric titration data can also be analyzed in terms of the Gibbs free energy required for the transfer of a proton from the polyanion to the bulk solution. The pK_a of any polyanions can be written as the sum of two contributions[19]

$$\mathrm{p}K_a = \mathrm{p}K_0 + 0.4343\frac{\mathrm{d}G_{el}}{RT\mathrm{d}\alpha} \quad (5)$$

where R is the gas constant and T is the absolute temperature. The first term in the equation, pK_0, is the contribution from the intrinsic dissociation constant that represents the dissociation of a proton from an isolated acid group. The pK_0 term can be obtained from the extrapolation of the pK_a curve to α = 0. Furthermore, it should also be independent of polymer composition. As observed from Figure 3B, the pK_a curves of the four polymers merged at α = 0, giving a pK_0 value of around 5.5. The second term in the equation, dG_{el}/dα, is a contribution from the electrostatic attraction between the H^+ and the existing COO^- at α > 0, and hence represents the extra work to dissociate H^+ from the polyanions.[20−22] The total extra energy for proton dissociation can be performed by separating the pK_0 term and carrying out graphical integration from α = 0 to 1 (eq 6). The cumulative extra Gibbs free energy with α for the four different polymers was then plotted in Figure 4.

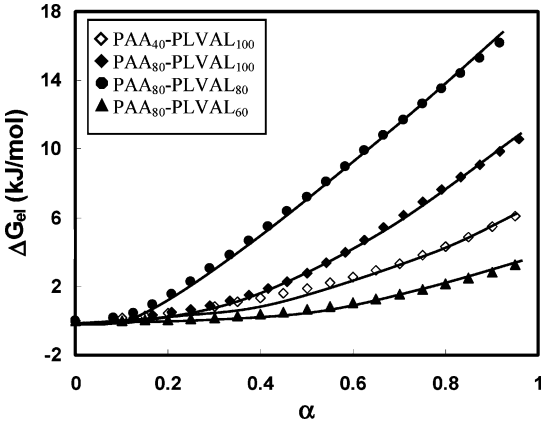

Figure 4. Comparison of total ΔG_{el} for PAA_{40}−$PLVAL_{100}$, PAA_{80}−$PLVAL_{100}$, PAA_{80}−$PLVAL_{80}$, and PAA_{80}−$PLVAL_{60}$.

$$\Delta G_{el} = 2.30RT\int_0^1 [\mathrm{p}K_\alpha - \mathrm{p}K_0]\mathrm{d}\alpha \quad (6)$$

From Figure 4, it can be observed that the total ΔG_{el} of the three PAA_{80}−$PLVAL_y$ polymers varied significantly from 2 to 16 kJ/mol. Since the length of the PAA segment in the three polymers was identical, the observed extra Gibbs free energy must not be entirely electrostatic in nature. One possible source that contributed toward ΔG_{el} was the capability of COOH groups to undergo hydrogen bonding with amide groups on the PLVAL segment.[17] Formation of these COOH−amide hydrogen bonds reduced the proportions of free COOH groups, as they became buried/intercalated within the hydrophobic domains of the self-assembled structure, rendering them inaccessible. Neutralization of these COOH groups, then, required the simultaneous breaking of COOH−amide hydrogen bonds and/or the rearrangements of hydrophobic domains, both of which required additional energy and hence will contribute to the large differences in the ΔG_{el} of the four polymers. This rearrangement of β-sheet hydrophobic domain of block copolymer systems with increasing solution pH was previously reported for both PAA_{80}−$PLVAL_y$ systems, where a larger β-sheet ordering occurred at intermediate pH due to the release of intercalated PAA chains, followed by destabilization of the β-sheet structure at high pH induced by charge repulsion.[17] The higher ΔG_{el} observed when the length of the PLVAL segment was reduced from 100 to 80 for the PAA_{80}−$PLVAL_y$ system was due to the increased probability for the formation of PAA−PLVAL hydrogen bonds, whereas the lowest ΔG_{el} in the PAA_{80}−$PLVAL_{60}$ system was due to the inability of the system to form well-defined aggregates

Table 2. Summary of Light Scattering and Circular Dichroism Data for $PAA_{80}-PLVAL_{80}$, $PAA_{80}-PLVAL_{100}$, and $PAA_{40}-PLVAL_{100}$ (pH 5−10)

polymer	α	R_h (nm)	R_g (nm)	R_g/R_h	$A_2 \times 10^{-4}$ (cm^3 mol/g^2)	total β-sheet (%)	aggregation number
$PAA_{80}-PLVAL_{80}$	0.10	67.8	30.7	0.54	−14.10	50.7	16
	0.17	70.9	44.6	0.58	−1.51	50.8	15
	0.26	87.2	58.0	0.73	0.95	43.2	16
	0.50	88.6	61.0	0.73	1.32	40.3	14
	0.75	86.3	61.3	0.76	7.84	38.6	15
	1.00	89.3	61.4	0.78	16.10	30.3	15
$PAA_{80}-PLVAL_{100}$	0.12	75.7	45.5	0.52	−21.80	55.0	32
	0.30	76.8	48.7	0.67	−16.50	56.1	31
	0.44	80.9	61.8	0.70	−3.22	50.6	32
	0.54	97.2	73.9	0.72	0.84	44.2	33
	0.75	98.6	77.7	0.74	3.52	42.9	31
	1.00	95.2	76.5	0.70	10.75	35.1	33
$PAA_{40}-PLVAL_{100}$	0.29	244	212.0	0.89	−41.60	62.5	392
	0.54	160	137.0	0.87	−20.10	56.7	336
	0.79	134	108.0	0.81	−15.50	48.4	282
	0.90	130	103.0	0.79	−15.10	38.8	212
	0.94	124	94.8	0.76	−8.70	35.7	141
	1.00	116	86.4	0.74	−1.05	35.3	117

either because of a lack of hydrophobicity or because of a lack of β-sheet formation and/or stability.[17]

Self-Assembly Behavior of PAA-*b*-PLVAL. The size, shape, and pH of the self-assembled morphology of the polymers were examined using dynamic and static light scattering techniques. In DLS, samples of varying pH and concentrations were measured at multiple scattering angles. The average diffusion coefficients at specific solution conditions (pH and polymer concentration) were then calculated and subsequently used to estimate the apparent hydrodynamic radius of the particles using the Stokes−Einstein equation

$$R_h = \frac{kT}{6\pi\eta D} \tag{7}$$

where k is Boltzmann's constant, T is temperature, η is solvent viscosity, and D is the diffusion coefficient of the particle. Additional micellar parameters, such as aggregation number, second virial coefficient (A_2), and radius of gyration (R_g), were obtained from SLS. In this case, the time-averaged intensities of scattered light were measured at different angles and at different concentrations. The SLS data were then analyzed based on the Debye equation

$$\frac{KC}{R(q)} = \frac{1}{\mathrm{MW}}\left(1 + \frac{1}{3}R_g{}^2q^2\right) + 2A_2C \tag{8}$$

where K is an instrument optical parameter ($K = 4\pi^2 n_{tol}{}^2(dn/dc)^2/N_A\lambda^4$, where n_{tol} is the refractive index of toluene (1.494), dn/dc is the refractive index increment of the polymer solution, N_A is Avogrado's number, and λ is the laser wavelength), C is the solution concentration, MW is the average molecular weight of the aggregates, and $R(q)$ is the absolute excess time-averaged scattered intensity (Rayleigh ratio). On the basis of the equation, the calculation of micellar parameters can be facilitated by replotting the SLS data of different polymers in the form of a Berry plot where $(KC/\Delta R(\theta))^{1/2}$ was plotted against $(\sin^2(\theta/2) + kC)$, with k being an adjustable constant. Extrapolation of the experimental data to zero concentration and zero angle gave us the micellar parameters of MW, R_g, and A_2.

A summary of the light scattering results for $PAA_{80}-PLVAL_{80}$, $PAA_{80}-PLVAL_{100}$, and $PAA_{40}-PLVAL_{100}$ is shown in Table 2, where the aggregation number is defined as the number of polymer chains per micelle and was calculated as the ratio of the micelle molecular weight (from SLS) and molecular weight of the polymer. Also shown are the changes in the total β-sheet content of the three block copolymer systems as reported previously.[17]

At the measured pH conditions, all three polymers exhibited an equilibrium with the coexistence of unimers and micelles (two DLS scattering peaks). Furthermore, the observed micelle size was independent of polymer concentration up to 0.1 wt %, which suggested that the self-assembly is via the closed-association mechanism. It can be observed from the table that water was a poor solvent for the polymer aggregates at low pH (negative A_2 values) and that the solvent quality improved progressively with increasing pH. It should be noted, however, that the polymer aggregates at all pH ranges were stable, despite the negative A_2 values, and hence, this showed the effectiveness of even a small amounts of charge to induce the dissolution of β-sheet containing aggregates. The observed trend for A_2 of the three polymers at the same degree of deprotonation (α) was reflective of their relative hydrophobicity, which increased with an increasing PLVAL/PAA molar ratio (i.e., $PAA_{40}-PLVAL_{100}$ > $PAA_{80}-PLVAL_{100}$ > $PAA_{80}-PLVAL_{80}$).

The ratios of R_g and R_h data from the light scattering data for $PAA_{80}-PLVAL_{100}$ and $PAA_{80}-PLVAL_{100}$ systems were found to be within 0.5−0.78 at all degrees of deprotonation (i.e., α (Table 2)). This was close to a maximum R_g/R_h ratio of 0.774 as theoretically determined for core−shell micellar systems from geometrical considerations. Therefore, the polymer systems self-assembled into core−shell micelles containing a hydrogen bonded β-sheet hydrophobic core, as confirmed by CD measurements,[17] and a PAA hydrophilic corona shell. The lower R_g/R_h ratio observed at the lower pH for these two polymers showed that the weight distribution of the core−shell micelle was concentrated toward the core, and hence, the micellar core was in a more condensed/collapsed state than at the higher pH conditions. The more compact micellar core was expected since the system sought to reduce the exposure of the hydrophobic region as the water−polymer interaction became poorer at low α as was indicated by the more negative A_2 at low α conditions.

The R_h and R_g data for $PAA_{80}-PLVAL_{80}$ and $PAA_{80}-PLVAL_{100}$ from Table 2 were plotted in terms of degree of deprotonation in Figure 5A,B respectively. The overall micelle size, as measured from the hydrodynamic radius (R_h), of $PAA_{80}-PLVAL_{100}$ was found to be larger than $PAA_{80}-PLVAL_{80}$ at all ranges of pH, and this difference can be attributed mainly to the difference in the PLVAL segment

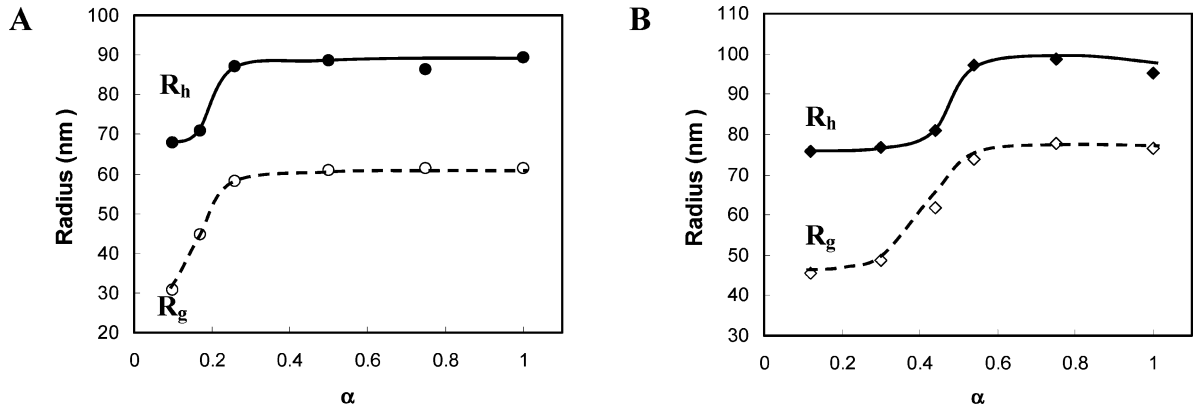

Figure 5. Effects of pH to the hydrodynamic (R_h) and gyration (R_g) radius of (A) $PAA_{80}-PLVAL_{80}$ and (B) $PAA_{80}-PLVAL_{100}$.

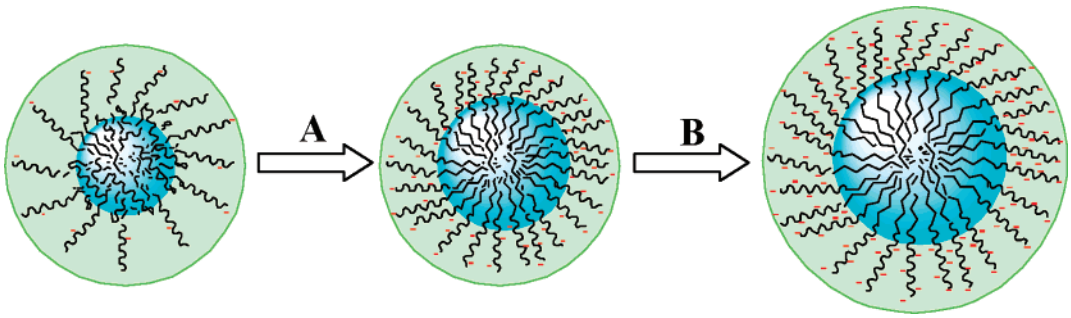

Figure 6. pH effects to micelle size of PAA80−$PLVAL_y$ systems (y = 80 or 100): inner blue circle and outer green circle representing changes in R_g and R_h, respectively. (A) Release of intercalated PAA at intermediate pH accompanied by increase of R_g and PAA density on the micelle shell and (B) swelling of micelle at high pH (concurrent increase of R_g and R_h) with the maximum degree of swelling determined by the balance between the tolerable increase of surface electrostatic repulsion and the inevitable loss of favorable hydrogen bonds at high degrees of swelling.

length. It should be noted that the observed changes in both R_h and R_g with pH for the two systems were not accompanied by a change in the aggregation number of the systems (cf. Table 2). Therefore, these changes were due mainly to the rearrangement of individual polymeric chains within the core−shell micelles to accommodate changes in pH without significantly altering the overall micellar composition and molecular weight.

Two additional observations can be made from Figure 5A,B. First, the two systems exhibited pH-responsive behavior that was similar to chemically cross-linked systems where a substantial increase of R_h occurred only at a relatively narrow α range, of 0.15 to 0.2 and 0.4 to 0.5 for $PAA_{80}-PLVAL_{80}$ and $PAA_{80}-PLVAL_{100}$ respectively, after which the micelle size remained constant. The observed increase in R_h for the two polymers at the narrow pH range can be attributed to the increase in the polymer charge density, which required the expansion of PAA segments over a larger area to minimize the effects of charge repulsions. At higher pH, however, the expansion was opposed by the consequential loss of favorable hydrogen bond interactions within the hydrophobic core. In this way, the multiple hydrogen bonds in the β-sheet structure act as physical cross-link points, which were sufficiently strong to maintain the overall size and shape of the micelles.

Another interesting feature that can be observed from Figure 5A,B was that the micellar radius of gyration (R_g) began to increase at a lower α during which the overall micelle size (R_h) remained constant (e.g., an increase of R_g was already observed at α = 0.1−0.15 and α = 0.3−0.4 for $PAA_{80}-PLVAL_{80}$ and $PAA_{80}-PLVAL_{100}$, respectively). Since the overall micelle size (R_h) remained constant in this α range, the observed increase in R_g suggested that the segmental chains redistributed within the micelle, possibly due to the decoupling of hydrogen bonds between PAA and PLVAL chains. This supported the previous hypothesis from potentiometric titration and CD observations[17] that there was an intercalation of PAA chains within the ordered hydrophobic PLVAL cores. The subsequent release of these intercalated segments then increased the PAA density in the micellar shell without any change in the overall size, which consequently caused the weight distribution in the micelle to shift outwardly toward the shell and increased the R_g.

Figure 6 provides an illustration on how the self-assembly of the $PAA_{80}-PLVAL_{80}$ and $PAA_{80}-PLVAL_{100}$ systems were affected by changes in pH based on the different observations from the light scattering and potentiometric titration experiments.

Having discussed the similarities between $PAA_{80}-PLVAL_{80}$ and $PAA_{80}-PLVAL_{100}$ systems, there were slight differences in the self-assembly of these two polymers. As can be observed from Figure 5, the α range for the change of R_h and R_g was different. The PLVAL segment in $PAA_{80}-PLVAL_{100}$ was longer and hence was capable of forming a more stable and tighter alignment of polymeric chains shown by a higher β-sheet content of approximately 5%. Therefore, it will require a higher pH to disrupt the β-sheet structure as illustrated in Figure 6. The additional effect of changing the degree of β-sheet formation through a change in PLVAL segment length can also be evaluated in terms of the shape regularity of the core−shell micelles. Figure 7A−C shows the TEM images of the $PAA_{80}-PLVAL_y$ systems (y = 60, 80, 100) at α of 1.

It is obvious from the TEM images that formation of ordered β-sheet structures was required for the shape regularity of the core−shell micelles with $PAA_{80}-PLVAL_{100}$ exhibiting the most regular spherical shape. Also included in the figure was the TEM image of random aggregates formed by $PAA_{80}-PLVAL_{60}$. It was interesting to note that the observed large structures were composed of much smaller capsule-like structures, which supported the two-step association process indicated by the surface tension measurement (filled triangles in Figure 2A). The small capsule structures were possibly comprised of a few

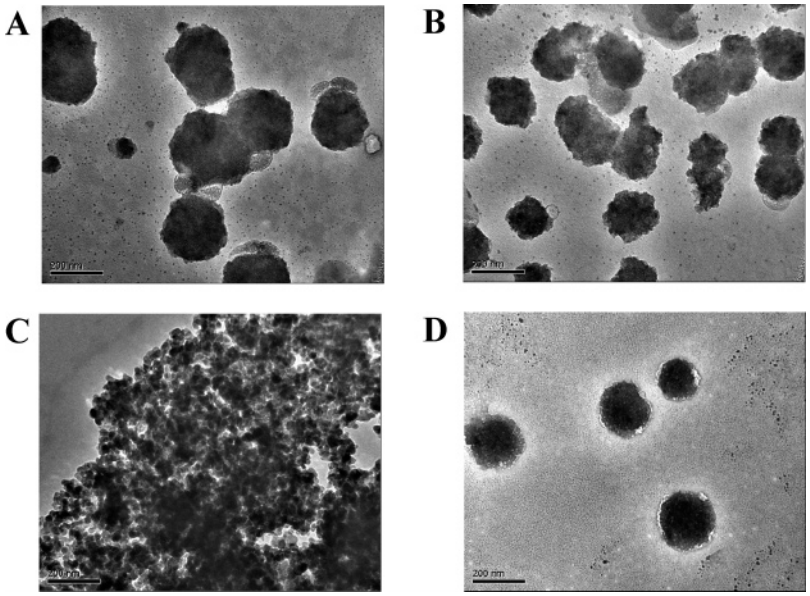

Figure 7. Effect of extent of β-sheet formation to the regularity of core−shell micelles in $PAA_{80}-PLVAL_y$ systems at 0.1 wt %. (A−C) Effects of decreasing PLVAL/PAA molar ratio at $\alpha = 1$ for $PAA_{80}-PLVAL_{100}$, $PAA_{80}-PLVAL_{80}$, and $PAA_{80}-PLVAL_{60}$, respectively. (D) Increase in regularity of core−shell micelles of the $PAA_{80}-PLVAL_{80}$ system at lower α ($\alpha = 0.3$, pH = 5).

polymer chains that cannot form an extended association, either in β-sheet form or hydrophobic association, due to its short PLVAL segment. These capsule structures, however, were unstable due to the exposure of hydrophobic PLVAL segments and will undergo further association in a random manner to form larger aggregates that eventually precipitated from solution. Further evidence of the role of the β-sheet on the regularity of core−shell micelles can be obtained by comparing the TEM images of $PAA_{80}-PLVAL_{80}$ at high and low α, as shown in Figure 7B,D, respectively. Concurrent with the improved extent of ordered β-sheet formation at lower pH as reported previously (Table 2),[17] it could be observed that the spherical structure in Figure 7D was better defined and with a lower polydispersity. Therefore, we concluded that the formation of this β-sheet structure was an important driving force in the micellization of block copolymer systems into regular core−shell spherical micelles.

Effects of PAA Segment Length on the Self-Assembly of PAA-*b*-PLVAL. The role of PAA segment in the self-assembly of the polymers can be evaluated by comparing the $PAA_{80}-PLVAL_{100}$ system with the $PAA_{40}-PLVAL_{100}$ system, where the PAA segment length of the latter was only half that of the former. The light scattering results of the $PAA_{40}-PLVAL_{100}$ system are summarized in Table 2 and plotted as a function of α in Figure 8. Also included in the figure was the plot of the distribution of relaxation times of the particles at different pHs.

Unlike the $PAA_{80}-PLVAL_{100}$ system discussed previously, it can be observed that there was a significant increase in R_g and R_h for the $PAA_{40}-PLVAL_{100}$ system at low α (Figure 8A), and this was accompanied by a broadening of the particle size distribution and the reduction of the fast unimeric peak (Figure 8B). Since the aggregation number of the system was also observed to increase (Table 2), these changes may be attributed to a possible change in the aggregate morphology. In particular, the geometrical R_g/R_h ratio was also observed to increase to 0.89 at lower pH, close to the theoretical value of 1 expected for vesicle structure. Examination of the TEM image of $PAA_{40}-PLVAL_{100}$ at low pH in Figure 9A, however, did not reveal the formation of any hollow structures, and the self-assembly still resembled a uniform spherical structure as was found at high pH, albeit with a higher polydispersity in the particle sizes.

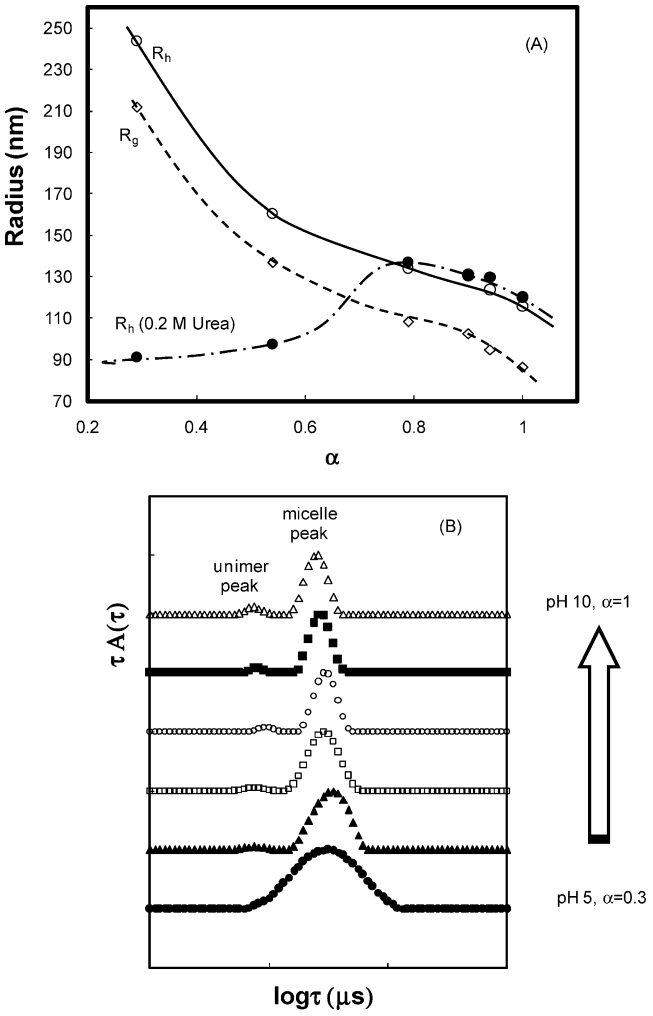

Figure 8. Light scattering analysis of $PAA_{40}-PLVAL_{100}$. (A) Effects of pH on the hydrodynamic (R_h) and gyration (R_g) radius and (B) effects of pH on the distribution function of particle relaxation times.

To probe the mechanism responsible for the morphological changes that occurred in the $PAA_{40}-PLVAL_{100}$ system due to changes in α, urea ($CO(NH_2)_2$) was added to the system. It was

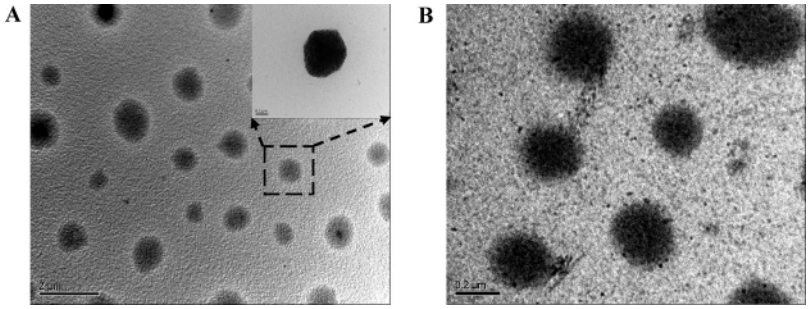

Figure 9. TEM image of 0.1 wt % $PAA_{40}-PLVAL_{100}$. (A) Formation of large and polydispersed spherical particles at $\alpha = 0.3$ and (B) effects of 0.2 M urea to the size and regularity of particles at $\alpha = 0.3$.

found that the presence of even a small amount of urea (i.e., 0.2 M) was sufficient to reduce the particle size from 245 to 90 nm at $\alpha = 0.3$ (Figure 8A). It can also be observed from the figure that urea addition impacted the particle size only at the low α region with no impact at the high α region. Further, it was also observed that the R_h trend as plotted in the figure did not change with further increases of the urea concentrations up to 1.1 M after which the polymer aggregates were completely dissociated and no particles could be observed in the light scattering. The TEM image of the $PAA_{40}-PLVAL_{100}$ system at 0.2 M urea and α of 0.3 is shown in Figure 9B. As compared to Figure 9A, it can be observed that the formed particles in the presence of urea were more uniform and also smaller in size.

Since urea is known to be a strong denaturant agent for the disruption of hydrogen bonds, the change in the polymer self-assembly must have originated from the formation of a more extended network of hydrogen bonds when the pH was reduced. However, these light scattering measurements alone could not determine the type of hydrogen bond network since both PAA and PLVAL segments contributed to the hydrogen bond formation at low pH. The circular dichroism measurements for $PAA_{40}-PLVAL_{100}$ at different urea concentrations had been previously reported, where the total β-sheet content in the core of the $PAA_{40}-PLVAL_{100}$ micelles remained essentially undisturbed by urea addition up to 0.2 M.[17] Therefore, we concluded that the observed large $PAA_{40}-PLVAL_{100}$ particles at low α (Figure 8A) were not just larger core−shell particles or vesicles due to the higher tendency of formation of extended β-sheet structures but were more likely to be large networks composed of a number of smaller collapsed micelles that were physically cross-linked by intermicellar hydrogen bonds. Figure 10 illustrates the proposed structure of these micellar networks, also known as compound micelles.

As illustrated in Figure 10, the intermicellar cross-links could be formed by hydrogen bonds between PAA segments in the shell of the micelles. Alternatively, the formation of the compound micellar structures may also be related to the existence of exposed regions of the hydrophobic core due to the shorter PAA segment length. The accessibility of hydrophobic cores of the $PAA_{40}-PLVAL_{100}$ system was previously concluded from CD measurements in the presence of urea, where at $\alpha = 0.3$, disruption of its β-sheet structure commenced at a lower urea concentration of 0.3 M as compared to 0.4 and 0.5 M for the $PAA_{80}-PLVAL_{100}$ and $PAA_{80}-PLVAL_{100}$ systems.[17] At low pH, the polymer micelles minimized these exposed regions by further association into a compound micellar structure, either through hydrogen bonding with PAA (PAA−PLVAL hydrogen bonds) or with exposed regions of neighboring micelles (PLVAL−PLVAL hydrogen bonds). Further, the partial exposure of the hydrophobic core was also evident from

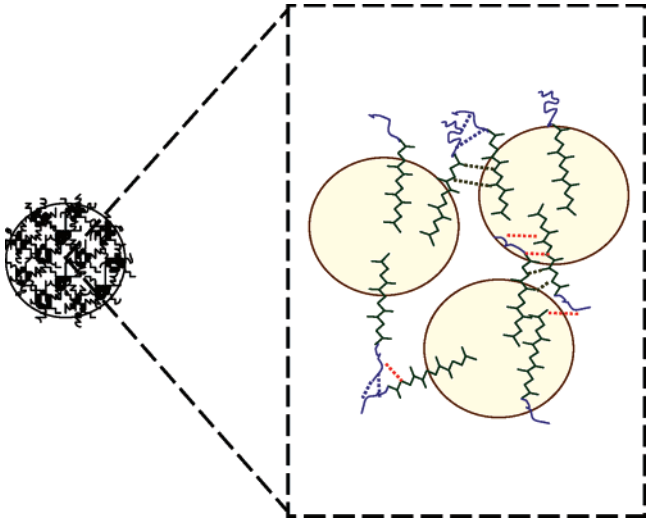

Figure 10. Formation of compound micelle structures through PAA−PAA hydrogen bonds (blue dotted lines), exposed PLVAL−PLVAL hydrogen bonds (black dotted lines), and PAA-exposed PLVAL hydrogen bonds (red dotted lines).

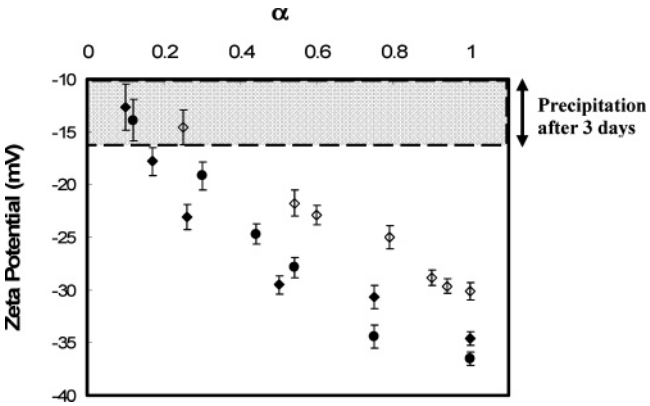

Figure 11. Determination of particle surface charge and stability for $PAA_{40}-PLVAL_{100}$ (◇), $PAA_{80}-PLVAL_{100}$ (◆), and $PAA_{80}-PLVAL_{80}$ (●).

the A_2 parameter of the system (Table 2), which remained negative even at high pH.

The aqueous stability and solubility of core−shell micelles formed by the three block copolymer systems were related to the surface charge density of particles, which can be evaluated by zeta potential measurements. Figure 11 shows the plot of zeta potentials as a function of α for the three polymers. In general, a more negative zeta potential was observed at higher α due to the deprotonation of COOH groups on PAA, and this was accompanied by the stabilization of the particles, which remained constant after a long period of time (up to 1 month). The trend of zeta potential and particle stability did not differ

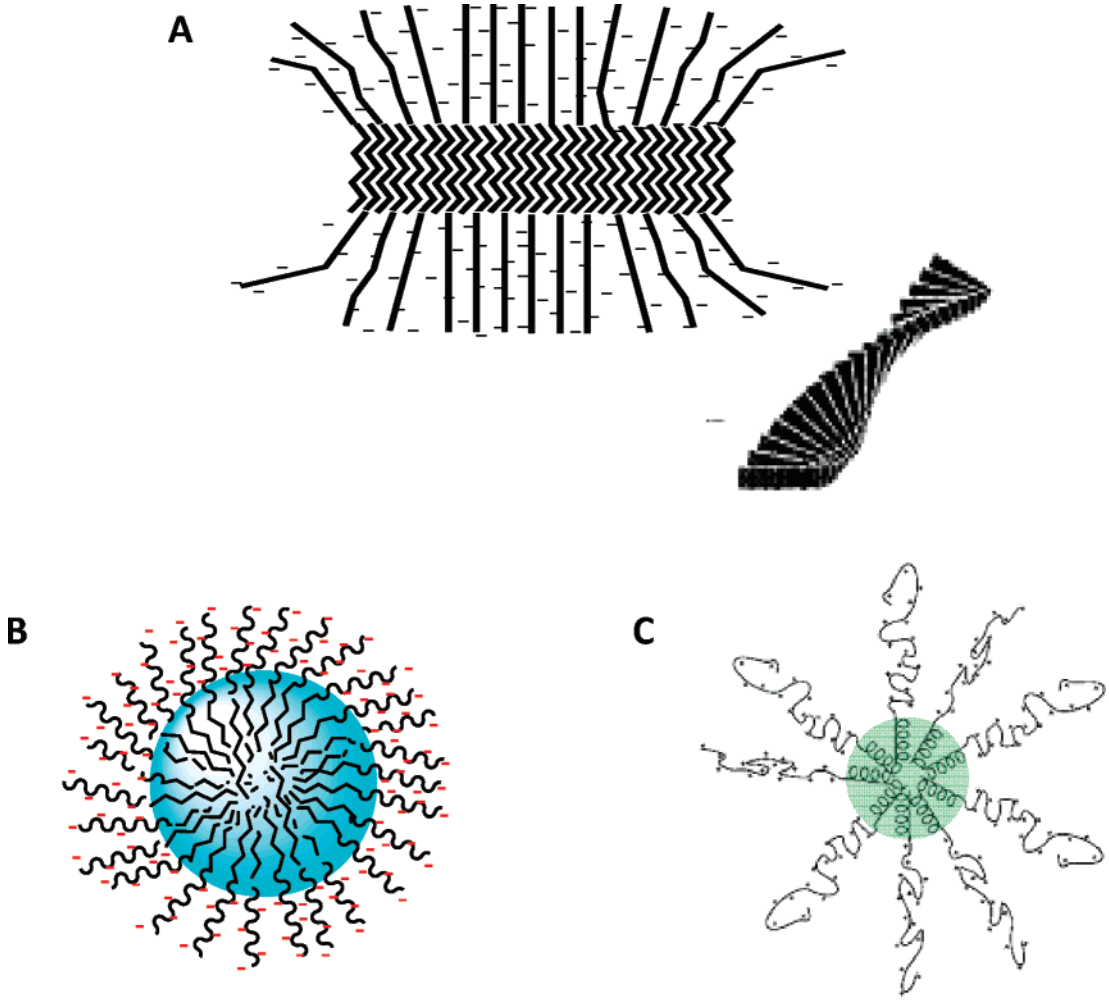

Figure 12. Diagram of potential molecular arrangements as a compromise between secondary structure formation and excluded volume/electrostatic effects of the polyelectrolyte segment. Panels A and B show the twisted fibril and core−shell arrangement in the PAA-*b*-PLVAL system, respectively.[9,10] Panel C shows a hypothetical core−shell arrangement for α-helix containing systems (e.g., K_x−L_y or E_x−L_y systems).

significantly for the PAA_{80}−$PLVAL_{80}$ and PAA_{80}−$PLVAL_{100}$ systems. A reduction in the length of the PAA segment to 40 units for PAA_{40}−$PLVAL_{100}$ resulted in a reduction of surface charge at all α and ultimately reduced the particle stability, where the system precipitated immediately at α slightly lower than 0.3 (pH < 5), while the precipitation for the two PAA_{80}−$PLVAL_y$ systems was only observed at a lower α of 0.1−0.2 (pH < 4). Therefore, the length of PAA was directly correlated with the solubilization and stability of the particles.

Molecular Mechanism in the Self-Assembly of PAA-*b*-PLVAL Polymers. The present study on the self-assembly of PAA-*b*-PLVAL systems is the first comprehensive study for a class of hybrid block copolymer system between a hydrophobic poly(L-amino acid) and a charged synthetic polymer. A similar system of amphiphilic copolypeptides containing a charged polypeptide segment (e.g., poly(lysine) −(K) or poly(glutamic acid) −(E)) and a hydrophobic leucine segment (K_x−L_y or E_x−L_y systems) was reported by Nowak and co-workers.[9] Heterogeneous hydrogel structures with a low critical gelation concentration that depended on the formation of an α-helical secondary structure by hydrophobic leucine residues affected by the leucine/lysine molar ratio were produced.[9] Since the amino acid residues of the PLVAL segment were as hydrophobic as the leucine residues in the K_x−L_y or E_x−L_y systems, they were expected to further associate into extended networks due to the formation of β-sheet secondary structures. It was interesting to observe that all four PAA-*b*-PLVAL systems examined in this study produced only core−shell spherical micellar structures.

Similar to the K_x−L_y systems, the formation of a long-range flat lamella arrangement was not favorable since it limits the volume available to the PAA segment, especially when its length is comparable or larger than the hydrophobic segment (steric or excluded volume effect). Moreover, an increase in the electrostatic repulsion from negative charges on the PAA segment to this two-dimensionally constrained arrangement will be more energetically unfavorable as compared to when the COO^- groups are allowed to spread out as far away as possible. Nowak and co-workers proposed that the charge repulsion of polyelectrolyte segments can be accommodated by the introduction of surface curvature either through the formation of a spherical structure (both core−shell and vesicle-like) or through the formation of ribbon-like twisted fibrils with the polyelectrolyte segment relaxing laterally. The latter was the dominant structure for K_x−L_y or E_x−L_y systems, and it allowed for the formation of the observed three-dimensional gels through the association of the exposed hydrophobic regions in the edges of the fibril structures. The formation of spherical vesicles was also observed by Nowak and co-workers when there was a reduced tendency of secondary structure formation in the K_x−L_y or E_x−L_y systems (e.g., when a lower leucine/lysine or leucine/glutamic acid molar ratio was used).[9]

Figure 12 illustrates the different possible structural arrangements for PAA-*b*-PLVAL systems in analogy with K_x−L_y or

E_x-L_y systems. It should be noted that unlike the K_x-L_y and E_x-L_y systems, the formation of core−shell spherical structures for PAA-*b*-PLVAL systems was possible since they did not experience the same geometrical restrictions as were observed for K_x-L_y and E_x-L_y systems, which formed intramolecular α-helices that subsequently acted as rigid rod-like building blocks. As can be seen in Figure 12C, packing of these rigid rods in a core−shell arrangement was not efficient and resulted in the existence of water pockets within the core and hence was energetically unfavorable. β-Sheet structure formation, on the other hand, is an intermolecular process and hence can accommodate closer packing of polymeric chains, allowing for the formation of core−shell structures. The high curvature needed for the spherical outline of the micelles was likely to result from the offset positioning between neighboring polymer chains instead of a perfect end-to-end alignment of polymer chains. This was also indicated by the substantial random coil content in the systems, which varied from 40% at pH 5 to around 70% at pH 10.

The exclusive formation of core−shell micelles for the PAA-*b*-PLVAL systems showed that it was a more thermodynamically stable arrangement as compared to the fibrillar structure. As compared to a core−shell structure, it can be thought that the fiber formation resulted in a much higher long-range structural ordering and reduced chain mobility, both of which were associated with a degree of entropic loss that was larger than the possible enthalpic gain from the more extensive β-sheet formation and from the minimization of strain toward the β-sheet that would exist in a core−shell arrangement. Hence, the core−shell structure was preferred for the PAA-*b*-PLVAL systems.

Conclusion

The aqueous self-assembly of novel block copolymers between poly(acrylic acid) and a poly(L-valine) was described for four different polymer compositions, namely, $PAA_{40}-PLVAL_{100}$, $PAA_{80}-PLVAL_{100}$, $PAA_{80}-PLVAL_{80}$, and $PAA_{80}-PLVAL_{60}$. The systems formed core−shell spherical micelles, whose core exhibited local ordering through the formation of a β-sheet structure of the PLVAL segment. The presence of this ordered structure resulted in an unusual pH behavior of the micelles, where an increase of the particle size occurred in a narrow α range (e.g., between 0.15 and 0.2 and 0.4 and 0.5 for $PAA_{80}-PLVAL_{80}$ and $PAA_{80}-PLVAL_{100}$, respectively), with the β-sheet inhibiting further swelling of micelles by accommodating the increased charge repulsive effects at high α. In addition, a higher extent of β-sheet structure formation was important for the shape regularity of the spherical micelles. $PAA_{80}-PLVAL_{60}$, with the lowest β-sheet content (approximately 12%) existed as unstable random aggregates at pH < 5 and in an unaggregated state at higher pH.

The length of PAA segment in the block copolymer systems was found to alter the self-assembly process at low pH, where insufficient shielding of hydrophobic core by shorter PAA chains in $PAA_{40}-PLVAL_{100}$ resulted in further micellar association into large compound micelles. The length of PAA segment was also important in improving the aqueous stability of the particles by increasing the negative charge density on the micellar shells.

Acknowledgment. We thank Dr. Ravi for his help in the developmental stage of the block copolymer synthesis and Dr. Rupert and Wu Binhui from the School of Biological Sciences, NTU for their assistance with the circular dichroism experiments. The authors thank the Singapore−MIT Alliance for financial support.

References and Notes

(1) Tan, J. F.; Too, H. P.; Tam, K. C. *Langmuir* **2006**, *22*, 3744.
(2) Xiong, X. Y.; Tam, K. C.; Gan, L. H. *J. Controlled Release* **2005**, *103*, 73.
(3) Gallot, B. *Prog. Polym. Sci.* **1996**, *21*, 1035.
(4) Gallot, B.; Hassan, H. H. *ACS Symp. Ser.* **1989**, *384*, 116.
(5) Klok, H. A.; Schlaad, H. *Adv. Polym. Sci.* **2006**, *202*, 53.
(6) Choucair, A.; Eisenberg, A. *Eur. Phys. J. E* **2003**, *10*, 37.
(7) Cornelissen, J. J. L. M.; Rowan, A. E.; Nolte, R. J. M.; Sommerdijk, N. A. J. M. *Chem. Rev.* **2001**, *101*, 4039.
(8) Lowik, D. W. P. M.; van Hest, J. C. M. *Chem. Soc. Rev.* **2004**, *33*, 234.
(9) Breedveld, V.; Nowak, A. P.; Jun Sato Deming, T. J. *Macromolecules* **2004**, *37*, 3943.
(10) Holowka, E. P.; Pochan, D. J.; Deming, T. J. *J. Am. Chem. Soc.* **2005**, *127*, 12423.
(11) Rodriguez-Hernandez, J.; Lecommandoux, S. *J. Am. Chem. Soc.* **2005**, *127*, 2026.
(12) Lawrence, B. A.; Vierra, C. A.; Mooref, A. M. F. *Biomacromolecules* **2004**, *5*, 689
(13) Jin, H. J.; Kaplan, D. L. *Nature (London, U.K.)* **2003**, *424*, 1057.
(14) Winningham, M. J.; Sogah, D. Y. *Macromolecules* **1997**, *30*, 862.
(15) Rathore, O.; Sogah, D. Y. *J. Am. Chem. Soc.* **2001**, *123*, 5231.
(16) Zhou, C.; Leng, B.; Yao, J.; Jie, Q.; Xin, C.; Ping, Z.; Knight, D. P.; Shao, Z. *Biomacromolecules* **2006**, *7*, 2415.
(17) Sinaga, A.; Hatton, T.A.; Tam, K.C. *Biomacromolecules* **2007**, *8*, 2801.
(18) Sinaga, A.; Ravi, P.; Hatton, T. A.; Tam, K. C. *J. Polym. Sci., Part A: Polym. Chem.* **2007**, *45*, 2646.
(19) Wang, C.; Ravi, P.; Tam, K. C.; Gan, L. H. *J. Phys. Chem. B* **2004**, *108*, 1621.
(20) Dubin, P.; Strauss, U. P. *J. Phys. Chem.* **1970**, *74*, 2842.
(21) Dubin, P.; Strauss, U. P. *J. Phys. Chem.* **1973**, *77*, 1427.
(22) Barone, G.; Virgilio, N. D.; Elia, V.; Rizzo, E. *J. Polym. Sci.* **1974**, *44*, 1.

MA071539L